Journal of Materials Chemistry A

Accepted Manuscript

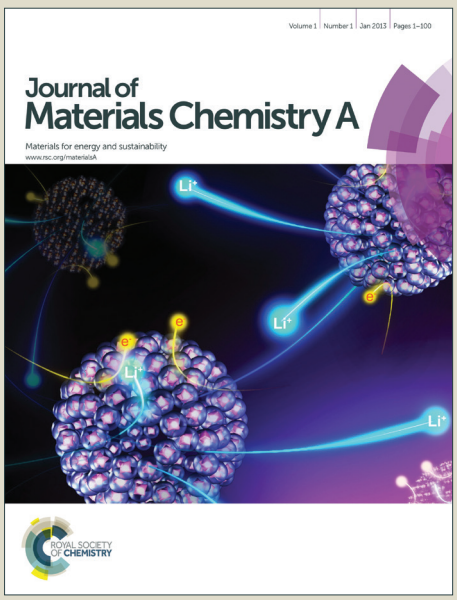

This is an *Accepted Manuscript*, which has been through the Royal Society of Chemistry peer review process and has been accepted for publication.

Accepted Manuscripts are published online shortly after acceptance, before technical editing, formatting and proof reading. Using this free service, authors can make their results available to the community, in citable form, before we publish the edited article. We will replace this *Accepted Manuscript* with the edited and formatted *Advance Article* as soon as it is available.

You can find more information about *Accepted Manuscripts* in the Information for Authors.

Please note that technical editing may introduce minor changes to the text and/or graphics, which may alter content. The journal's standard Terms & Conditions and the Ethical guidelines still apply. In no event shall the Royal Society of Chemistry be held responsible for any errors or omissions in this *Accepted Manuscript* or any consequences arising from the use of any information it contains.

ROYAL SOCIETY OF CHEMISTRY

www.rsc.org/materialsA

Cite this: DOI: 10.1039/c0xx00000x

www.rsc.org/xxxxxx

ARTICLE TYPE

Ultrathin and High-Ordered CoO Nanosheet Arrays for Lithium-Ion Batteries with High Cycle Stability and Rate Capability†

Dongdong Li, Liang-Xin Ding,* Suqing Wang, Dandan Cai and Haihui Wang*

Received (in XXX, XXX) Xth XXXXXXXXX 20XX, Accepted Xth XXXXXXXXX 20XX

DOI: 10.1039/b000000x

Ultrathin and high-ordered 2D CoO nanosheet arrays (NSAs) composed of nanocrystals were fabricated via a facile galvanostatic electrodeposition technique. The as-prepared CoO NSAs exhibit excellent cycleability (retain 1000 mA h g^{-1} after 100 cycles at 1 A g^{-1}) and rate capability (520 mA h g^{-1} at 10 A g^{-1}) when they are directly used as an anode for LIBs.

Lithium storage of the anode is one of the key technologies to develop next generation high-performance lithium-ion batteries (LIBs).[1] Currently, the commercialized graphite-based anode materials exhibit excellent charge and discharge cycling performance, but their low specific capacity can't satisfy the demand for high energy density batteries.[2] So it is necessary to develop new anode materials with higher capacity to replace the low specific capacity of graphite. Up to now, various materials, such as non-graphitic carbon,[3, 4] metal oxides,[5, 6] chalcogenides,[7] nitrides,[8] lithium alloys and their composites,[9] have been exploited as potential anode materials for high-performance LIBs. Among them, metal oxides, such as CoO_x,[10-14] Fe_xO_y,[15, 16] $InVO_4$,[17] SnO_2,[18] TiO_2,[19] Fe_3BO_6[20] and CuO,[21, 22] are considered as the most promising anode materials because of their high theoretical specific capacities (in general multiple times higher than those of carbon/graphite-based materials).[5] Especially CoO, owing to its completely reversible electrochemical reaction mechanism, is becoming one of the most appealing anode materials for LIBs.[11, 14, 23, 24]

However, the practical use of metal oxides as anodes in LIBs is also facing some intractable problems. Most of the studied metal oxides belong to semiconductors, which usually exhibit poor ion/electrical transport kinetics and quite detrimental as electrode materials. Moreover, metal oxides inevitably suffer from pronounced volume change during the Li^+ insertion/extraction processes, and consequently resulting in a large irreversible capacity loss and poor cycling stability.[6] In order to overcome these barriers, many appealing strategies have been proposed, including the use of carbon-based nanocomposites[12, 25-27] and unique nanostructures such as core-shell nanoparticles,[28] nanorods,[29] nanotubes,[30] nanowires,[31] and nanosheets,[15, 32] etc. Although these efforts can signally shorten the paths for lithium ion diffusion and offer more active surface for electrode reaction, they only play a very limited role in improving the electronic conductivity of metal oxides due to the weak interfacial connection among nanomaterials and the addition of ancillary materials. In addition, the easily damaged structure of nanomaterials during the cycle processes would inevitably lead to a degree of capacity fading. As a result, their rate capability and cycling stability are still not satisfactory. Therefore, it is imperative to further enhance the electron conduction and structural stability of metal oxides to achieve their practical application in LIBs.

Recently, self-supported and binder-free one-dimensional (1D) and/or two-dimensional (2D) metal oxide nanoarrays are of great interest in LIBs[10, 33-35] and supercapacitors[36-38] because of their enhanced electron transportation capability and low ionic diffusion resistance compared with their bulk counterparts. A typical example is the self-supported 1D/2D cobalt oxide nanoarrays including nanowires,[10, 24, 39] nanotubes[40] and nanosheets[41-46] have been successfully prepared and all exhibited enhanced electrochemical performance. Particularly, the nanoarray electrodes with porous configuration not only can accelerate lithium ion diffusion, but also can effectively buffer volume change during the charge/discharge processes.[10, 40] Based on the above observations, it is reasonably deducible that cobalt oxide nanoarrays with ultrathin, polycrystalline and interconnected nanosheet structures possibly can endow better electrochemical characteristics, such as higher electroactive materials utilization, more convenient electronic transmission path and better electrochemical stability, which interestingly, correspond exactly to the requirement for metal-oxide-based electrode materials in LIBs. Thus, it is highly desirable to synthesize the mentioned cobalt oxide nanosheet arrays for LIBs application. Approaching this purpose, many synthesis methods have been used to prepare cobalt oxide/hydroxide nanosheet arrays electrode materials, such as hydrothermal,[42] chemical precipitation,[45] molten salt,[47, 48] carbothermal reducation[49] and electrodeposition.[41, 43, 44] Among all these synthesis methods, researchers have demonstrated that electrodeposition is the most effective way to synthesise 2D metal oxides/hydroxide nanosheet arrays owing to its template-free and direct growth pattern on a conductive substrate. Nevertheless, the electrodeposition method, which has been reported in the literature, is mainly based on the use of potentiostatic electrodeposition technique. Due to the changing deposition current in the deposition process, the difficulties involved in controlling the homogeneous nucleation and growth direction of the nanosheets on a conductive substrate, it is difficult to obtain ultrathin (<10 nm) and highly ordered nanosheet arrays structure. So the development of simple and effective methods to synthesize the high-quality 2D nanosheet arrays is still considered to be a challenging task.

Herein, we introduce a facile galvanostatic electrodeposition technique to controllable synthesize ultrathin and high-ordered 2D CoO nanosheet arrays (NSAs) on a porous nickel foam substrate. The synthesis involves the galvanostatic electro-deposition of $Co(OH)_2$ on the substrate and subsequent thermal transformation to CoO, which is illustrated in Scheme 1. Notably, this high-quality hierarchical architecture as an attractive design for LIBs electrode can: *i*) provide a 3D highway network for fast

Journal of Materials Chemistry A Accepted Manuscript

electron transport and thus obviously improve the electrical conductivity of the overall electrode; *ii*) provide large active surface area and rich nanopores for the high-efficiency electrochemical reaction and fast electrolyte penetration/diffusion; *iii*) form a pleasant flexible structure to resist the volume expansion-contraction during cycling; *iv*) grow directly on the porous nickel foam substrate and does not require the additional polymer binder and coating process. Due to the above-mentioned advantages which originated from the integration of the novel nanosheet arrays architecture, the as-synthesized CoO NSAs exhibit superior electrochemical performance when they are directly used as an anode for LIBs.

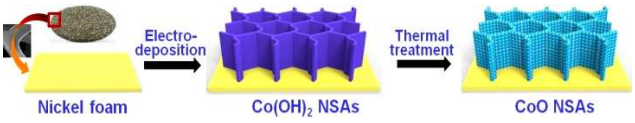

Scheme 1 Schematic illustration for the fabrication of CoO NSAs.

Fig. S1 shows the EDX pattern of the initial dark green deposit. The strong spectral peaks of Co and O suggest that the cobalt or cobalt-oxide-based compounds have a successful deposition on the nickel foam substrate. The XRD result in Fig. 1a demonstrated that the as-prepared deposits can be primarily identified as a pure phase of $Co(OH)_2$ with a hexagonal structure (JCPDS no. 30-0443). Furthermore, it is also found that the diffraction peaks of $Co(OH)_2$ disappeared in the XRD pattern (Fig. 1b) after a thermal treatment at 200 ^oC for 3 h, and the peaks at 2θ values of 37.0^o, 43.4^o appeared instead, which can be indexed to a face-centered cubic structure of CoO (JCPDS no. 48-1719), showing a successful conversion of the precursor $Co(OH)_2$ to CoO.

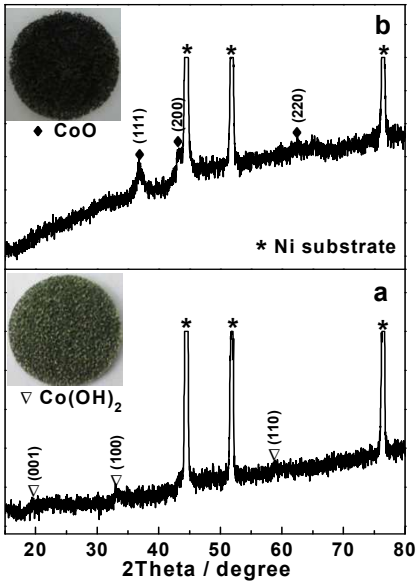

Fig. 1 XRD patterns of the as-prepared deposits (a) before and (b) after thermal treatment.

To further probe the changes of the chemical composition and the valence state of the as-prepared deposits before and after thermal treatment. XPS measurements were carried out. Fig. 2a and b show XPS spectra of the Co 2p and O 1s core levels obtained from the initial $Co(OH)_2$ deposit and the final CoO product, respectively. As shown in Fig. 2a, the Co $2p_{3/2}$ and Co $2p_{1/2}$ peaks of the $Co(OH)_2$ deposit are observed at binding energies of 781.6 and 797.3 eV, which are characteristic of a $Co(OH)_2$ phase. Similarly, there are two major peaks also observed in the Co 2p spectrum of the CoO product. Here it is clearly seen that the two peaks can be deconvoluted into two pairs of doublets. Apparently, the peaks located at binding energy of 780.2 and 795.2 eV are assigned to CoO phase.[50] Meanwhile, the presence of the two smaller shoulder peaks at 781.8 and 796.8 eV should be attributed to the small amount of residual $Co(OH)_2$. From Fig. 2b, it is seen that the O 1s XPS spectra of the two samples all can be deconvoluted into three sub-peaks. The peaks located at binding energy of 530.0 and 531.2 eV are assigned to O bond in CoO crystalline networks and OH bond in $Co(OH)_2$ crystalline networks, respectively, while the other three smaller peaks can be assigned to the weakly absorbed surface hydroxyl (531.8 eV) and structural water (531.8 eV).[51] The significantly reduction of the intensity of OH bond peak at 531.2 eV and the new presentation of O bond peak at 530.0 eV further indicate that the precursor $Co(OH)_2$ can be successful converted into the CoO by a thermal treatment at 200 ^oC for 3 h.

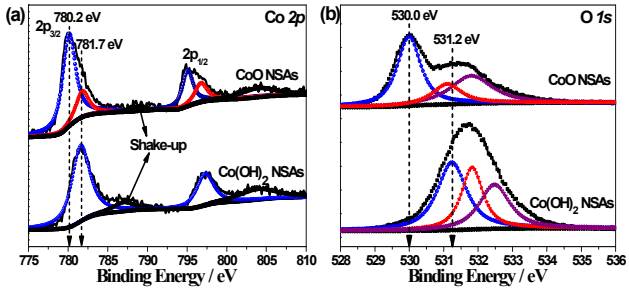

Fig. 2 XPS spectra of (a) Co 2p and (b) O 1s performed on the as-prepared deposits before and after thermal treatment.

The morphology of the as-synthesized CoO product was primarily examined by SEM. The typical SEM image viewed from the top is shown in Fig. 3a. It can be observed that the CoO nanosheets are uniformly grown on the nickel foam substrate and have an ordered growth behavior. The magnified SEM image in Fig. 3b shows that these CoO nanosheets are regularly interconnected with each other and are almost vertically grown on the nickel foam substrate, forming a typical 2D nanosheet arrays (NSAs) structure. The further magnified SEM image is shown in the inset of Fig. 3b, which shows that the CoO nanosheets have a smooth surface and the thicknesses of the nanosheet is about 10 nm. In addition, it should be pointed out that, compared to the precursor of $Co(OH)_2$ nanosheets (Fig. S3), the morphology of the CoO nanosheets is almost not altered after the thermal treatment.

The morphology and structure of the as-synthesized CoO NSAs were further investigated by TEM. Fig. 3c shows a typical TEM image of the as-synthesized CoO NSAs, which provides a relatively large range of top-view. The interconnected and uniform ridge-like characteristic with a clearly dark/light contrast are strongly suggested the existence of an ordered nanosheet-array structure. Obviously, the observations were in accordance with the SEM images mentioned above. The magnified TEM images are shown in Fig. 3d and Fig. S4, which reveal that the CoO nanosheets are porous and consist of the homogeneous overlapped nanocrystals with a size ranging from 4 to 5 nm. Moreover, it can be seen that the thickness of the nanosheets is about 8 nm, which is in good agreement with SEM observations above. The selected area electron diffraction (SAED) pattern inserted in Fig. 3c shows a set of diffraction rings, which further indicate that CoO nanosheets are polycrystalline and small size characteristics. Examination of an individual nanocrystal with high-resolution TEM (Fig. 3d, inset) indicates that it is highly crystalline along its entire particle and a considerably lattice

Journal of Materials Chemistry A Accepted Manuscript

This journal is © The Royal Society of Chemistry [year]

fringe with spacing of 0.21 nm is very consistent with the value of the (200) plane of cubic CoO. The N_2 adsorption/desorption isotherms of the CoO NSAs are shown in Fig.S5. The BET specific surface area of the CoO NSAs is calculated to be 179.5 $m^2 g^{-1}$, which is much higher than that of previously reported Co-oxides.[48, 52] Moreover, a typical IV-type hysteresis loop is observed which indicates that the CoO NSAs has a porous structure. The pore size distribution curve (the inset in Fig. S5) shows that the majority pore size is about 2.7 nm. Therefore, from the composition and structural analysis, it is certain that a temperature of 200 ^oC is enough for the conversion of $Co(OH)_2$ to CoO and make it well-crystallized. Notably, the unique 2D nanoarray architecture of the CoO nanosheets along with their polycrystalline and porous structure characteristics will be able to provide enormous opportunities for enhancing their functions and application performance. For instance, the provided large open space and convenient channels which are very beneficial to accelerating species diffusion and electron transportation, and thus enhancing their electrochemical performance.

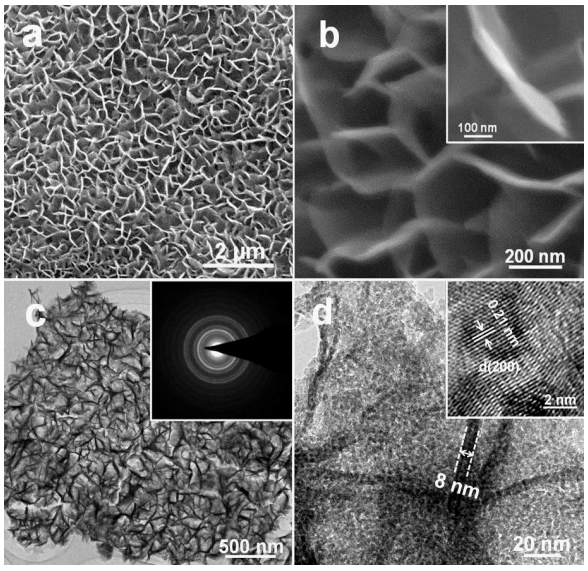

Fig. 3 (a, b) SEM; (c) TEM and SAED (inset); and (d) HRTEM images of CoO NSAs.

Inspired by the attractive 2D nanosheet arrays architecture, the CoO NSAs were tested as an electrode for LIBs. Fig. 4a shows cyclic voltammograms of the CoO NSAs at a scanning rate of 0.2 mV s^{-1} in a voltage range of 0.01-3.0 V vs. Li/Li^+. It is clear from the CV curves that there is a sharp peak at 0.8 V in the first cathodic scan. While in the subsequent cycles, the peak has a positive shift of the potential about 0.1 V and a decrease of density, in additional, a new cathodic peak appears at 1.4 V. The difference of the cathodic peaks between the first and subsequent cycles is mainly related to the irreversible reactions with the electrolyte. In the anodic scans, two peaks at 1.5 and 2.2 V are recorded. The peak at 2.2 V is corresponded to the oxidation of Co to form cobalt oxide accompanying Li^+ extraction which is in agreement with the previous reports,[53] and the peak at 1.5 V is due to the oxidation of Ni.[54]

Fig. 4b shows the galvanostatic discharge/charge voltage profiles of the CoO NSAs electrode cycled at a current density of 1 A g^{-1} within the voltage range of 0.01-3.0 V vs. Li/Li^+. A broad plateau around 1.0 V is observed in the first discharge curve, which shifts to higher voltage and becomes less well-defined in the subsequent cycles. Meanwhile, two sloping plateaus at the range of about 1.2-1.7 V and 2.0-2.5 V appear in the first charge curve, and are stable in the subsequent cycles. Notably, these features are in good qualitative agreement with the CV results in Fig. 4a. In addition, it is also observed that the first discharge/charge capacities are 1062.0 and 836.5 mA h g^{-1}, respectively, indicating the irreversible capacity loss of about 21%. It is well accepted that the irreversible capacity is attributed to the formation of a solid electrolyte interphase films during the first discharge process.[55, 56] Moreover, the discharge/charge capacities are higher than the theoretical capacity of CoO (715 mA h g^{-1}) which have been reported by some papers, [57, 58] due to the participation of excess oxygen in the nano-sized CoO sample，[57]and extra interfacial Li storage and the reversible decomposition of the electrolyte with the formation of SEI while cycling.[5] It is noticed that the CoO NSAs electrode exhibits a relatively high initial discharge/charge capacities and a smaller irreversible capacity loss compared with the reported cobalt-oxide-based LIBs anode materials,[11, 14] which indicate the CoO nanosheets with a 2D array structure have a significantly improved lithium-storage performance.

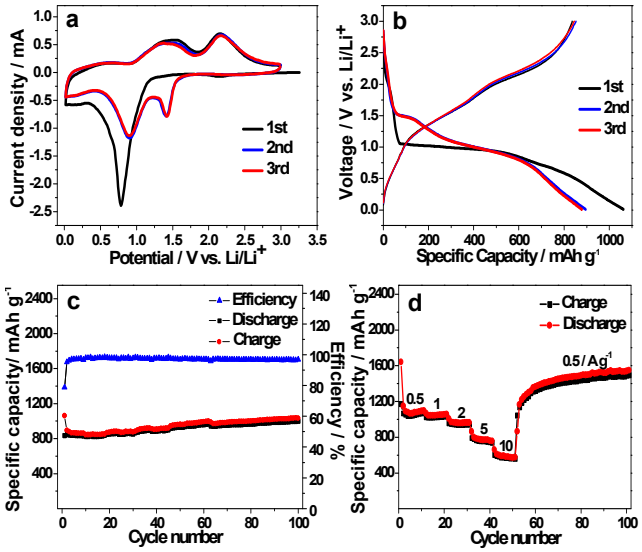

Fig. 4 (a) CV curves of the CoO NSAs at a scan rate of 0.2 mV s^{-1}. (b) Discharge and charge voltage profiles of the CoO NSAs at a current density of 1 A g^{-1}. (c) Cycling performance of the CoO NSAs at a current density of 1 A g^{-1} and (d) at various current densities of 0.5, 1, 2, 5, 10 A g^{-1}. All carried out in the voltage range 0.01-3.0 V vs. Li/Li^+.

Fig. 4c gives the cycling performance of the CoO NSAs electrode at a constant current density of 1 A g^{-1}. It is found that the reversible capacities show an upward trend with the cycles and reach 1000 mA h g^{-1} after 100 discharge/charge cycles. Meanwhile, the coulombic efficiency has been maintained at 96% after the second cycle, indicating the high lithium storage capability and the excellent cycling stability of the CoO NSAs. These desirable results can be ascribed to the unique nanosheet arrays structure which is benificial to increase the electrochemical activity and effectively resist the volume expansion during cycling. Moreover, the phenomenon of the gradual increased capability of the CoO NSAs, which has been well-documented in the literature, is attributed to the extra interfacial Li storage and the reversible decomposition of the electrolyte with the formation of polymeric gel-like film.[11]

To further demonstrate very high electrochemical performance of the CoO NSAs, the rate capability of the CoO NSAs is also investigated. Fig. 4d shows the rate capability of the CoO NSAs at the current densities between 0.5 and 10 A g^{-1}, which clearly indicate that the synthesized CoO NSAs exhibit a favourable

Journal of Materials Chemistry A Accepted Manuscript

reversible capacity at every current density. In particular, even the current density reaches 10 A g^{-1}, the CoO NSAs still exhibits a considerable specific capacity of 560 mA h g^{-1}, 52.8% of the initial capacity, indicating the excellent rate capability. To our knowledge, this is the best reported rate capability for cobalt-oxide-based LIBs anode materials. Here we also find that, after the high current density measurements, the specific capacity of the as-prepared CoO is very similar to the cycling performance at the current density of 1 A g^{-1} (Fig. 4c), showing a clear increasing trend with the cycles. After the 100 cycles, the reversible capacity of 1495 mA h g^{-1} is achieved, which further corroborates the excellent rate capability and cycling stability of the synthesized CoO NSAs.

The excellent electrochemical performance of the synthesized CoO NSAs, especially the excellent rate capability and cycling stability, should be associated with not only the efficient nickel foam current collector, but also the designed morphology. More specifically, the establishment of the interconnected nanosheets array directly grown on the high-quality nickel foam current collector with a good solid contact can form a stable and highly conducting 3D highway network that will make the electrons rapidly conducted back and forth from the CoO nanoparticles to the current collector, and thus markedly improving the rate performance. Besides, the ultrathin CoO nanosheet with the polycrystalline and small size characteristics can provide high electrochemically active surface area, as well as a large number of nanopores, which will facilitate electrolyte diffuse into the inner of the CoO nanosheets and make almost all of CoO nanoparticles expose as electroactive sites. Meanwhile, the formation of the uniform nanopores in CoO nanosheets can provide lots of elastic buffer space to accommodate the volume changes during the lithium ion insertion/extraction, which is in favor of the cycle stability.

Conclusions

In summary, the ultrathin and high-ordered CoO NSAs were successfully fabricated on nickel foam substrate using a facile galvanostatic electrodeposition technique with subsequent thermal transformation process. The as-prepared CoO NSAs as an advanced anode material for LIBs exhibited superior electrochemical performance, especially the excellent cycleability (retain 1000 mA h g^{-1} after 100 cycles at 1 A g^{-1}) and rate capability (520 mA h g^{-1} at 10 A g^{-1}), making CoO NSAs a promising anode material for high power LIBs. The superior electrochemical performance should be attributed to the combination of several favourable factors of the designed morphology including fast electronic transportation highways, high stability flexible structure and large active surface area. Furthermore, the results of this study also provide new insight into the use of galvanostatic electrodeposition technique to controllable synthesize high-quality metal-oxide-based electrode materials, which can be used to achieve improved performance in LIBs.

Acknowledgements

This work was supported by National Science Fund for Distinguished Young Scholars of China (no. 21225625) and the Pearl River Scholar Program of Guangdong Province.

Notes and references

School of Chemistry & Chemical Engineering, South China University of Technology, No. 381 Wushan Road, Guangzhou 510640 (China). Fax: (+86)20-87110131; E-mail: lxding@scut.edu.cn, hhwang@scut.edu.cn

† Electronic Supplementary Information (ESI) available: Experimental details, EDX patterns of $Co(OH)_2$ NSAs and CoO NSAs, SEM image of $Co(OH)_2$ NSAs, HRTEM image of CoO NSAs, N2 adsorption/desorption isotherm of the CoO NSAs, XPS spectra of Ni 2p for $Co(OH)_2$ NSAs and CoO NSAs on the nickel foam substrates, and the analysis of the electrochemically active of the nickel foam electrode. See DOI: 10.1039/b000000x/

1. M. V. Reddy, G. V. Subba Rao and B. V. R. Chowdari, *Chem. Rev.* 2013, **113**, 5364-5457.
2. J.-M. Tarascon and M. Armand, *Nature* 2001, **414**, 359-367.
3. D. Pan, S. Wang, B. Zhao, M. Wu, H. Zhang, Y. Wang and Z. Jiao, *Chem. Mater.* 2009, **21**, 3136-3142.
4. L. Qie, W.-M. Chen, Z.-H. Wang, Q.-G. Shao, X. Li, L.-X. Yuan, X.-L. Hu, W.-X. Zhang and Y.-H. Huang, *Adv. Mater.* 2012, **24**, 2047-2050.
5. P. Poizot, S. Laruelle, S. Grugeon, L. Dupont and J. Tarascon, *Nature* 2000, **407**, 496-499.
6. J. Jiang, Y. Li, J. Liu, X. Huang, C. Yuan and X. W. D. Lou, *Adv. Mater.* 2012, **24**, 5166-5180.
7. J. W. Seo, J. T. Jang, S. W. Park, C. Kim, B. Park and J. Cheon, *Adv. Mater.* 2008, **20**, 4269-4273.
8. J. L. Rowsell, V. Pralong and L. F. Nazar, *J. Am. Chem. Soc.* 2001, **123**, 8598-8599
9. Y. Yu, C. H. Chen, J. L. Shui and S. Xie, *Angew. Chem. Int. Ed.* 2005, **44**, 7085-7089.
10. Y. Li, B. Tan and Y. Wu, *Nano Lett.* 2008, **8**, 265-270.
11. C. Peng, B. Chen, Y. Qin, S. Yang, C. Li, Y. Zuo, S. Liu and J. Yang, *ACS Nano* 2012, **6**, 1074-1081.
12. Z.-S. Wu, W. Ren, L. Wen, L. Gao, J. Zhao, Z. Chen, G. Zhou, F. Li and H.-M. Cheng, *ACS Nano* 2010, **4**, 3187-3194.
13. J. Wang, N. Yang, H. Tang, Z. Dong, Q. Jin, M. Yang, D. Kisailus, H. Zhao, Z. Tang and D. Wang, *Angew. Chem. Int. Ed.* 2013, **52**, 6417-6420.
14. Y. Sun, X. Hu, W. Luo and Y. Huang, *J. Phys. Chem. C* 2012, **116**, 20794-20799.
15. M. Reddy, T. Yu, C.-H. Sow, Z. X. Shen, C. T. Lim, G. Subba Rao and B. Chowdari, *Adv. Funct. Mater.*, 2007, **17**, 2792-2799.
16. B. Wang, J. S. Chen, H. B. Wu, Z. Wang and X. W. Lou, *J. Am. Chem. Soc.* 2011, **133**, 17146-17148.
17. M. V. Reddy, B. L. Wei Wen, K. P. Loh and B. V. R. Chowdari, *ACS Appl. Mater. Interfaces*, 2013, **5**, 7777-7785.
18. X. M. Yin, C. C. Li, M. Zhang, Q. Y. Hao, S. Liu, L. B. Chen and T. H. Wang, *J. Phys. Chem. C*, 2010, **114**, 8084-8088.
19. D. Wang, D. Choi, J. Li, Z. Yang, Z. Nie, R. Kou, D. Hu, C. Wang, L. V. Saraf and J. Zhang, *ACS Nano*, 2009, **3**, 907-914.
20. X. Shi, C. Chang, J. Xiang, Y. Xiao, L. Yuan and J. Sun, *J. Solid. State. Chem.*, 2008, **181**, 2231-2236.
21. J. C. Park, J. Kim, H. Kwon and H. Song, *Adv. Mater.*, 2009, **21**, 803-807.
22. M. V. Reddy, C. Yu, F. Jiahuan, K. P. Loh and B. V. R. Chowdari, *ACS Appl. Mater. Interfaces*, 2013, 5, 4361-4366.
23. C. Chen, B. Hwang, J. Do, J. Weng, M. Venkateswarlu, M. Cheng, R. Santhanam, K. Ragavendran, J. Lee and J. Chen, *Electrochem. Commun.* 2010, **12**, 496-498.
24. J. Jiang, J. Liu, R. Ding, X. Ji, Y. Hu, X. Li, A. Hu, F. Wu, Z. Zhu and X. Huang, *J. Phys. Chem. C* 2010, **114**, 929-932.
25. D. S. Su and R. Schlögl, *ChemSusChem* 2010, **3**, 136-168.
26. H. Wang, L. F. Cui, Y. Yang, H. Sanchez Casalongue, J. T. Robinson, Y. Liang, Y. Cui and H. Dai, *J. Am. Chem. Soc.*, 2010, **132**, 13978-13980.
27. S. Yang, X. Feng, S. Ivanovici and K. Müllen, *Angew. Chem. Int. Ed.* 2010, **49**, 8408-8411.
28. M. G. Kim, S. Sim and J. Cho, *Adv. Mater.* 2010, **22**, 5154-5158.
29. Y.-M. Lin, P. R. Abel, A. Heller and C. B. Mullins, *J. Phys. Chem. Lett.* 2011, **2**, 2885-2891.
30. N. Kang, J. H. Park, J. Choi, J. Jin, J. Chun, I. G. Jung, J. Jeong, J. G. Park, S. M. Lee and H. J. Kim, *Angew. Chem. Int. Ed.* 2012, **51**, 6626-6630.
31. L. Mai, L. Xu, C. Han, X. Xu, Y. Luo, S. Zhao and Y. Zhao, *Nano Lett.* 2010, **10**, 4750-4755.

Journal of Materials Chemistry A Accepted Manuscript

This journal is © The Royal Society of Chemistry [year]

32. J. W. Seo, Y. W. Jun, S. W. Park, H. Nah, T. Moon, B. Park, J. G. Kim, Y. J. Kim and J. Cheon, *Angew. Chem. Int. Ed.* 2007, **46**, 8828-8831.
33. J. Chen, X.-H. Xia, J.-P. Tu, Q.-Q. Xiong, Y.-X. Yu, X.-L. Wang and C.-D. Gu, *J. Mater. Chem.* 2012, **22**, 15056-15061.
34. M.-S. Wu and H.-W. Chang, *J. Phys. Chem. C* 2013, **117**, 2590-2599.
35. X. Xia, J. Tu, Y. Zhang, J. Chen, X. Wang, C. Gu, C. Guan, J. Luo and H. J. Fan, *Chem. Mater.* 2012, **24**, 3793-3799.
36. H. Wang, Y. Wang and X. Wang, *New J.Chem.* 2013, **37**, 869-872.
37. F. Yang, J. Yao, F. Liu, H. He, M. Zhou, P. Xiao and Y. Zhang, *J. Mater. Chem. A* 2013, **1**, 594-601.
38. Q. Li, Z.-L. Wang, G.-R. Li, R. Guo, L.-X. Ding and Y.-X. Tong, *Nano Lett.* 2012, **12**, 3803-3807.
39. K. T. Nam, *Science*, 2006, **312**, 885-888.
40. X. W. Lou, D. Deng, J. Y. Lee, J. Feng and L. A. Archer, *Adv. Mater.* 2008, **20**, 258-262.
41. L.-B. Kong, M.-C. Liu, J.-W. Lang, M. Liu, Y.-C. Luo and L. Kang, *J. Electrochem. Soc.* 2010, **15**, 571-577.
42. J. Zhu, Y. K. Sharma, Z. Zeng, X. Zhang, M. Srinivasan, S. Mhaisalkar, H. Zhang, H. H. Hng and Q. Yan, *J. Phys. Chem. C* 2011, **115**, 8400-8406.
43. Y. Fan, H. Shao, J. Wang, L. Liu, J. Zhang and C. Cao, *Chem.Commun.* 2011, **47**, 3469-3471.
44. J.-H. Zhong, A.-L. Wang, G.-R. Li, J.-W. Wang, Y.-N. Ou and Y.-X. Tong, *J. Mater. Chem.* 2012, **22**, 5656-5665.
45. Y. Wang, H. Wang and X. Wang, *Electrochim. Acta* 2013, **92**, 298-303.
46. C. Yuan, L. Yang, L. Hou, L. Shen, X. Zhang and X. W. D. Lou, *Energy Environ. Sci.* 2012, **5**, 7883-7887.
47. M. V. Reddy, Z. Beichen, L. J. e. Nicholette, Z. Kaimeng and B. V. R. Chowdari, *Electrochem. Solid-State Lett.*, 2011, **14**, A79-A82.
48. M. V. Reddy, Z. Beichen, K. P. Loh and B. V. R. Chowdari, *CrystEngComm*, 2013, **15**, 3568-3574.
49. M. V. Reddy, G. Prithvi, K. P. Loh and B. V. R. Chowdari, *ACS Appl. Mater. Interfaces*, 2014, **6**, 680-690.
50. R. Dedryvère, S. Laruelle, S. Grugeon, P. Poizot, D. Gonbeau and J. M. Tarascon, *Chem. Mater.*, 2004, **16**, 1056-1061.
51. J.-K. Chang, C.-M. Wu and I.-W. Sun, *J. Mater. Chem.* 2010, **20**, 3729-3735.
52. Y. Liu and X. Zhang, *Electrochim. Acta*, 2009, **54**, 4180-4185.
53. W. Yao, J. Yang, J. Wang and Y. Nuli, *J. Electrochem. Soc.*, 2008, **155**, A903-A908.
54. B. Varghese, M. Reddy, Z. Yanwu, C. S. Lit, T. C. Hoong, G. Subba Rao, B. Chowdari, A. T. S. Wee, C. T. Lim and C.-H. Sow, *Chem. Mater.*, 2008, **20**, 3360-3367.
55. T. Zheng, A. S. Gozdz and G. G. Amatucci, *J. Electrochem. Soc.* 1999, **146**, 4014-4018.
56. Y. S. Hu, R. Demir-Cakan, M. M. Titirici, J. O. Müller, R. Schlögl, M. Antonietti and J. Maier, *Angew. Chem. Int. Ed*. 2008, **47**, 1645-1649.
57. C. H. Chen, B. J. Hwang, J. S. Do, J. H. Weng, M. Venkateswarlu, M. Y. Cheng, R. Santhanam, K. Ragavendran, J. F. Lee, J. M. Chen and D. G. Liu, *Electrochem. Commun.*, 2010, **12**, 496-498.
58. X. Zheng, G. Shen, Y. Li, H. Duan, X. Yang, S. Huang, H. Wang, C. Wang, Z. Deng and B.-L. Su, *J. Mater. Chem. A*, 2013, **1**, 1394-1400.

Journal of Materials Chemistry A Accepted Manuscript